PHYSICAL REVIEW B **88**, 064106 (2013)

Possible origin of the discrepancy in Peierls stresses of fcc metals: First-principles simulations of dislocation mobility in aluminum

Ilgyou Shin
Department of Chemistry, Princeton University, Princeton, New Jersey 08544-1009, USA

Emily A. Carter[*]
Department of Mechanical and Aerospace Engineering, Program in Applied and Computational Mathematics and Andlinger Center for Energy and the Environment, Princeton University, Princeton, New Jersey 08544-5263, USA

(Received 24 March 2013; revised manuscript received 27 June 2013; published 28 August 2013)

Dislocation motion governs the strength and ductility of metals, and the Peierls stress (σ_p) quantifies dislocation mobility. σ_p measurements carry substantial uncertainty in face-centered cubic (fcc) metals, and σ_p values can differ by up to two orders of magnitude. We perform first-principles simulations based on orbital-free density functional theory (OFDFT) to calculate the most accurate currently possible σ_p for the motion of $\frac{1}{2}\langle 110\rangle\{111\}$ dislocations in fcc Al. We predict the σ_ps of screw and edge dislocations (dissociated in their equilibrium state) to be $1.9 \times 10^{-4}G$ and $4.9 \times 10^{-5}G$, respectively (G is the shear modulus). These values fall within the range of measurements from mechanical deformation tests (10^{-4}–$10^{-5}G$). OFDFT also finds a new metastable structure for a screw dislocation not seen in earlier simulations, in which a dislocation core on the glide plane does not dissociate into partials. The corresponding σ_p for this undissociated dislocation is predicted to be $1.1 \times 10^{-2}G$, which agrees with typical Bordoni peak measurements (10^{-2}–$10^{-3}G$). The calculated σ_ps for dissociated and undissociated screw dislocations differ by two orders of magnitude. The presence of undissociated, as well as dissociated, screw dislocations may resolve the decades-long mystery in fcc metals regarding the two orders of magnitude discrepancy in σ_p measurements.

DOI: 10.1103/PhysRevB.88.064106 PACS number(s): 61.72.Lk, 62.40.+i, 71.15.Mb

I. INTRODUCTION

Dislocation motion plays a critical role in plastic deformation of crystals. Dislocations, the carriers of plasticity, are ubiquitous in real materials. Their presence is responsible for shear strengths many orders of magnitude less than the theoretically predicted strength of a hypothetical defect-free crystal.[1] Dislocation mobility is quantified by the Peierls stress (σ_p), which is the minimum external stress required to move a stationary dislocation irreversibly at 0 K.

Interpreting σ_p measurements in face-centered cubic (fcc) metals has been challenging when studying metal plasticity. σ_p can be estimated experimentally from the critical resolved shear stress measured by a mechanical deformation test or from the Bordoni relaxation peak of an internal friction measurement,[2] where the Bordoni peak has been interpreted in terms of the thermally activated kink pair formation mechanism.[3] Both methods provide similar σ_p values in body-centered cubic (bcc) metals and NaCl- and CsCl-type ionic crystals. However, the two methods can differ by two orders of magnitude in fcc metals. For the σ_p of fcc Al, mechanical deformation tests yield estimates of 10^{-4}–$10^{-5}G$,[4] while the typical Bordoni peaks in internal friction measurements provide estimates of 10^{-2}–$10^{-3}G$.[5–8] Notably, a lower-temperature Bordoni peak corresponding to a σ_p of 10^{-4}–$10^{-5}G$ was observed more recently in ultra–high-purity, zone-refined Al.[9,10] This value, similar to those from mechanical tests, provides a clue of the true σ_p for a pure Al single crystal. Unfortunately, *in situ* measurements of the atomic-scale motion of dislocations are not yet possible. To discern what is occurring at that scale instead requires accurate computer simulations of dislocation motion in order to reconcile the long-lasting puzzle of the drastically differing σ_p measurements in fcc metals.

Numerous theoretical simulations have directly calculated σ_p to help elucidate plastic deformation mechanisms in fcc metals. These models can be divided into two groups: (1) direct atomic simulations using molecular dynamics (MD) and molecular statics and (2) indirect estimation of the σ_p from first-principles generalized stacking fault energies (GSFEs) based on the framework of the Peierls-Nabarro (PN) model.[1,11,12] Direct atomic simulations have used primarily the classical embedded atom method (EAM) interatomic potential,[13,14] since accurate quantum mechanics (QM) methods such as Kohn-Sham density functional theory (KSDFT)[15] are too computationally demanding for dislocation structure and motion simulations. The direct atomic simulations predict σ_ps for screw and edge dislocations within ranges of 1–82 and 1–13 MPa, respectively.[16–23] Indirect PN estimations generally yield much larger values for a screw dislocation (∼256 MPa) but similar values for an edge dislocation (∼1–3 MPa) compared to those from atomistic simulations[17,24–26] *(vide infra)*. Although the calculations fall within a large range of measurements—10^{-2}–$10^{-5}G$, where G is measured to be ∼25 GPa (Ref. 27)—it is not clear which simulation technique reliably models which experimental method.

EAM atomic simulations have achieved widespread success for modeling mechanical properties of simple metals and intermetallics. Their computational efficiency enables large-scale atomic simulations that account for inherent material relaxation properties. However, EAM potentials are not fully transferable, and their accuracy can suffer when modeling states of matter significantly different from those used in their original fitting. First-principles QM methods should be more transferable because each term in the energy expression is based on fundamental physical laws. Additionally, QM calculations can describe metal stacking fault energies (SFEs) more accurately than do EAM calculations.[28] The PN model, which bridges SFEs to dislocation core structures, is likely to be overly simplistic and does not account for atomic relaxation. What is needed is a sufficiently accurate QM method that is also fast enough to follow structural changes so that atomic simulations of dislocation motion can be run to extract reliable σ_ps. Orbital-free density functional theory (OFDFT) is a transferable first-principles QM method that can be made to scale linearly with system size.[29] It does so by directly solving for the electron density instead of introducing an auxiliary set of one-electron orbitals (as done in conventional KSDFT). Although KSDFT can be made to scale linearly for nonmetals,[30] a large prefactor for metals (due to the delocalized nature of electrons in metals) means large-scale calculations are still prohibitively expensive (unless extraordinary computing resources are used.[31]). By contrast, OFDFT permits more efficient atomic simulations of metals.[29,32–35]

OFDFT accuracy relative to KSDFT depends on the quality of two approximations beyond the usual electron exchange-correlation functional. One is the kinetic energy density functional (KEDF) used to evaluate the electron kinetic energy, and the second is the local pseudopotentials (LPPs) used when calculating the ion (screened nucleus)–valence electron interaction energy. Several OFDFT applications with state-of-the-art KEDFs[36–39] and transferable bulk-derived LPPs[40,41] reveal that OFDFT can describe many properties (e.g., equilibrium volumes and structures, relative phase stabilities, elastic constants, and SFEs[35,39,42–45]) of main group metals and semiconductors with comparable accuracy to KSDFT. For Al, complex mechanical phenomena, such as vacancy aggregation, deformation of nanowires, ductile processes at crack tips, and dislocation structures, have been successfully studied with OFDFT simulations,[28,46–49] lending credence to its use in what follows.

In this study, we first calculate the σ_p of $\frac{1}{2}\langle 110\rangle\,\{111\}$ screw and edge dislocations with OFDFT. In pure Al, such dislocations typically dissociate into two $\frac{1}{6}\langle 112\rangle\,\{111\}$ Shockley partials that bound a locally hexagonal close-packed (hcp) stacking fault (SF) region. We then compare the σ_p of the dissociated screw dislocation to that of a metastable, undissociated $\frac{1}{2}\langle 110\rangle\,\{111\}$ screw dislocation that we have found. Elasticity theory predicts that an undissociated screw dislocation can be in a metastable state when the equilibrium dislocation width is narrow ($<10b$, where b is the Burgers vector).[50] Al's dislocation width is indeed narrow ($\sim 4b$) due to its high SFE. However, the undissociated dislocation in Al has not been observed experimentally, since the narrow width makes it difficult to distinguish dissociated and undissociated core structures. The presence of this undissociated $\frac{1}{2}\langle 110\rangle\,\{111\}$ screw dislocation in Al, its structure, and its motion have not been reported previously. To the best of our knowledge, only OFDFT has found this metastable, undissociated core structure. As we shall show, the two possible dislocation core structures (dissociated and undissociated) are likely the origin of the two orders of magnitude discrepancy in the σ_p measurements.

II. COMPUTATIONAL DETAILS

We employ the climbing image nudged elastic band (CINEB) transition state search algorithm[51,52] within the OFDFT simulation to evaluate the minimum energy path (MEP) and energy barrier for dislocation motion. We then compare the CINEB prediction to atomic simulations under quasistatic loading conditions as another measure of σ_p.

Our linear scaling OFDFT method was presented in several previous papers.[29,48,53] All OFDFT calculations are carried out using PROFESS 2.0 (PRinceton Orbital-Free Electronic Structure Software), an open-source FORTRAN90 code developed by Carter and co-workers.[29,53]

We calculate electronic exchange and correlation (XC) using the local density approximation (LDA) derived from the quantum Monte Carlo results of Ceperley and Alder[54] as parameterized by Perdew and Zunger.[55] The LDA XC provides a good description of nearly-free-electron–like metals such as Al because it is exact for the uniform electron gas. The LDA XC typically overestimates binding energies and accordingly overestimates shear moduli and SFEs. However, since LPPs in OFDFT tend to underestimate SFEs[48] compared to those estimated from experiments,[56–59] we use the LDA XC, which should give better agreement with experiments due to error cancellation between the LDA and the LPP.

We treat the electron kinetic energy using the 1999 Wang-Govind-Carter (WGC99) nonlocal KEDF, which contains two universal density exponents $\alpha,\beta = \frac{5}{6} \pm \frac{\sqrt{5}}{6}$. The two-body Fermi wave vector mixing parameter γ is set to 2.7. This parameter set is optimal for main group metals.[38] The reference density ρ_* in the Taylor expansion of the WGC99 kernel is chosen to be the average electron density of equilibrium fcc Al. The nonlocal term of WGC99 KEDF may diverge in very low electron density (vacuum) regions that surround an isolated dislocation treated within periodic boundary conditions. Since the vacuum region should not physically contribute to any energy term evaluated via a density functional, we are free to neglect these spurious contributions. In order to numerically handle these artifacts, we multiply the diverging term by a smooth cutoff function[48]

$$f(r) = \frac{\exp\left\{\frac{\rho(r)}{D}\right\} - 1}{\exp\left\{\frac{\rho(r)}{D}\right\} + \exp\left\{\frac{\rho_c}{D}\right\}}, \tag{1}$$

where ρ_c is the cutoff density below which $f(r)$ goes to zero quickly and above which it approaches unity quickly. D controls the smoothness of $f(r)$ at ρ_c. We set $\rho_c = 10^{-5}$ and $D = \rho_c/10$.

We calculate the ion-electron interaction energy using a transferable bulk-derived local pseudopotential (BLPP). We generate the BLPP by inverting the Kohn-Sham (KS) equations to obtain the KS effective potential, using as input the densities of various phases containing different coordination numbers (fcc, bcc, simple cubic, and cubic diamond). We obtain each input density from KSDFT using a standard Troullier-Martins (TM) nonlocal pseudopotential (NLPP).[60] We derive the BLPP from the KS effective potential by unscreening the latter by the XC and Hartree potentials. This BLPP accurately approximates TM NLPP predictions of KSDFT electron densities in various Al structures. Detailed procedures for deriving BLPSs and the quality of the Al BLPS were reported previously.[40,41]

A plane wave basis kinetic energy cutoff of 600 eV sufficiently converges the total energy and the lattice parameter

TABLE I. Details of various supercells used in dislocation motion simulations.

Simulation method	Dislocation	No. of atoms	Crystallographic orientation	Cell size (Å × Å × Å)
CINEB MEP calculation	Screw	2112	X $[1\bar{1}2]$, Y $[1\bar{1}\bar{1}]$, Z $[110]$	$107.0 \times 110.1 \times 2.809$
	Edge	2982	X $[110]$, Y $[\bar{1}1\bar{1}]$, Z $[\bar{1}12]$	$101.1 \times 96.3 \times 4.866$
Quasistatic loading simulation	Screw	4224	X $[1\bar{1}2]$, Y $[1\bar{1}\bar{1}]$, Z $[110]$	$155.7 \times 151.4 \times 2.809$
	Edge	4482	X $[110]$, Y $[\bar{1}1\bar{1}]$, Z $[\bar{1}12]$	$118.0 \times 123.9 \times 4.866$

of fcc Al to within 0.03 meV/atom and 1.2×10^{-5} Å, respectively. It also converges dislocation core structures in terms of the partial splitting width, which did not change, even with a much larger basis in which the cutoff was increased to 1200 eV. Recall that k-point sampling and Fermi surface smearing are not used in OFDFT since there are no one-electron orbitals or energy levels but rather only a density and a total energy. For density optimizations, we use a truncated Newton method with a tolerance for the total energy convergence of 2.7×10^{-5} eV (1.0×10^{-6} Ha) so that the energy is well converged even for samples containing thousands of atoms.

We model dislocations based on an anisotropic linear elastic displacement field.[1] A dislocation core is built in the center of a rectangular super cell with one unit lattice vector periodically replicated along the dislocation line direction Z, thereby modeling an infinitely long dislocation line. Our supercell contains an even number of periodic unit cells along the X and the Y directions so that the initial core is located in the exact center of the periodic supercell. This initial condition produces the metastable undissociated core of the screw dislocation, as well as the more stable dissociated cores of the screw and edge dislocations. Table I provides details of the various simulation cells used in this work. The cell sizes given therein are large enough to converge the dislocation core structures (e.g., partial splitting widths) and energies; i.e., the structures and energies do not change with larger cell sizes. We use an isolated dislocation model in which 10 Å of vacuum between neighboring periodic slabs eliminates artificial interactions between periodic images. This vacuum layer thickness was verified to be sufficiently thick to produce converged results. As an alternative to the isolated dislocation model, we also considered quadrupolar arrays in which a surrounding vacuum layer is not needed in periodic supercells. However, the non-negligible interaction between neighboring, opposing dislocations in a moderately-sized cell significantly lowered the σ_p. Thus, we concluded that the isolated dislocation model provides more realistic physical properties.

We compare two boundary conditions for the surfaces normal to the X and Y directions (Table I). The first is a fixed boundary condition [Fig. 1(a)] where atoms within 6 Å of the surfaces are fixed at their initial positions (determined by elasticity theory) during ion relaxation to impose the correct far-field displacement boundary condition on the dislocation (this allows the dislocation to reside in bulk-like surroundings in the far field, where long-range elastic strain is dominant). The second is a mixed boundary condition [Fig. 1(b)] where atoms within 6 Å of the surface normal to the Y direction are fixed only in the normal direction; the other surface (normal to the glide direction X) is a free boundary to accommodate the glide of the dislocation. Isotropic linear elasticity theory estimates an image stress on the free surface as $\sigma_{img} \sim Gx^2/\pi d^2$ as the isolated single dislocation moves by one unit vector x along the glide plane, where G and d are respectively the shear modulus and the cell dimension. Hence, any calculated σ_ps of similar magnitude to this image stress could be questionable (*vide infra*). CINEB calculations impose both boundary conditions, while quasistatic loading simulations use only the mixed boundary condition to model deformation on the boundary of a moving dislocation.

As further verification of the robustness of these boundary conditions, we compared the positions of the boundary atoms built by elasticity theory for a perfect core vs Shockley partials to estimate how much the boundary atoms are affected by core dissociation. For the cell sizes listed in Table I, the maximum difference in atomic positions within the 6-Å constrained surface region was ∼0.00025 Å, suggesting that the cell size is large enough to describe both dissociated and undissociated cores within the fixed boundary condition without introducing misfit strain. (More boundary condition tests and test details are included as supplemental material.[61]) Furthermore, in our previous work examining Al dislocation structures,[48] we thoroughly benchmarked boundary conditions (a quadrupolar array of dislocations in a periodic boundary vs an isolated core in a constrained boundary) by comparing their predictions of the partial splitting width to the most recent experimental data.[62] The two boundary conditions predicted similar widths and were in reasonable agreement with experiment, which validates the isolated core model in a constrained boundary condition. Finally, we note that the constrained boundary condition is commonly used for simulating dislocation motion; see, for example, Ref. 63.

The first and last dislocation structures within CINEB simulations are optimized using the conjugate gradient (CG) method. We set the convergence threshold for the maximum force component on atoms to be 2.5 meV/Å (4.9×10^{-5} Ha/bohr). The distance between the dislocation core positions in the first and last structures is set to one periodic unit along the glide direction X. Fifteen replica images are constructed from a linear interpolation between the optimized first and last structures. Images are then optimized with a maximum force threshold of 5.0 meV/Å (9.8×10^{-5} Ha/bohr). For CINEB calculations with the undissociated screw dislocations, atoms within a 5-Å radius from the core are frozen in their interpolated positions. Not doing so causes CINEB calculations to not converge within the force tolerance. Imposing this constraint predicted slightly larger (∼1.2×) σ_p for the dissociated screw dislocations, where we could compare results with or without this constraint.

The close agreement between the results obtained from the two conditions suggests that imposition of this constraint is acceptable. The relative dislocation core energy $E_C(x)$ is calculated as

$$E_C(x) = E_{CINEB}(x) - E_{CINEB}(0) - \{E_{CINEB}(L) - E_{CINEB}(0)\} \cdot (x/L), \tag{2}$$

where $E_{CINEB}(x)$ is the total energy at x, the travel distance of the dislocation core, and L is one periodic unit. $\{E_{CINEB}(L) - E_{CINEB}(0)\} \cdot (x/L)$ averages the slight difference in the dislocation core energies of the two terminal CINEB images (this difference is negligible compared to the energy barrier ($\max|E_C(x)|$)). $E_C(x)$ is then interpolated so that its gradient *(vide infra)* can be calculated by numerical differentiation. Assuming the deformation occurs slowly enough to achieve a quasistatic equilibrium, then the stress $\sigma(x)$ applied to or experienced by the dislocation during its motion is given by[64]

$$\sigma(x) = \frac{1}{b^2}\frac{dE_c(x)}{dx}. \tag{3}$$

By definition, the Peierls stress is defined as

$$\sigma_p = \max|\sigma(x)|. \tag{4}$$

For the quasistatic loading simulations, we explicitly apply a shear stress along the Burgers vector to the supercell by shearing all atoms therein according to the strain field corresponding to this shear stress. We increase the shear strain and then relax the atoms based on the CG method with a maximum force threshold of 2.5 meV/Å (4.9×10^{-5} Ha/bohr). To estimate the σ_p, we repeat this procedure until the dislocation core starts to move from its strain-free position. Strain increments are $\Delta\varepsilon = 10^{-4}$ and 10^{-5} for the screw and edge dislocations, respectively; accordingly, the uncertainty of the calculation is the same as $\Delta\varepsilon$.

We identify dislocation cores based on the common neighbor analysis (CNA) pattern for each atom,[65] which is built in the LAMMPS MD code.[66] CNA can recognize five local structures: fcc, hcp, bcc, icosahedral, and "unknown." We assume that a dislocation core is located at the center of unknown structure atoms, implying a distorted region around the core.

III. RESULTS AND DISCUSSION

As stated earlier, experimentally measured and theoretically predicted σ_ps for fcc metals can differ by up to two orders of magnitude. Our first goal is to calculate the most accurate possible σ_ps to provide guidelines for computing σ_ps in metals and for evaluating the quality of previous simulation methods (Sec. III A). Our second goal is to explain the significant discrepancies of σ_ps measured and calculated for fcc metals. OFDFT atomic simulations show two screw dislocation core structures are possible, i.e., dissociated and undissociated cores. Their σ_ps differ by two orders of magnitude, which finally identifies the probable origin of the long-standing discrepancy in measured σ_ps (Sec. III B).

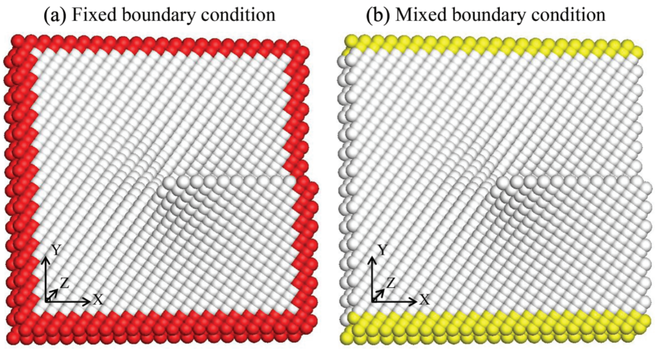

FIG. 1. (Color online) (a) Fixed and (b) mixed boundary conditions used for the screw and edge dislocation calculations listed in Table II. (Figures are drawn for a screw dislocation as an example, but an edge dislocation used the same fixed and mixed boundary conditions.) The supercell is rectangular. Atoms in red are fixed during ion relaxation. Atoms in yellow are fixed only in the Y direction. Atoms in gray are free to move in all directions. See text for details.

A. Peierls stresses of dislocations in fcc Al

1. *Results*

We optimize the position of each (nonfixed) atom in the supercell based on *ab initio* forces calculated using OFDFT. To the best of our knowledge, Al σ_p values have not been extracted previously from QM-based atomic simulations, so σ_p values from our OFDFT atomic simulations maybe the most accurate ones available. We compare two types of simulations with OFDFT: a CINEB construction of an MEP and a quasistatic loading simulation in which energy minimization of the structure is performed after each loading increment. We also compare two boundary conditions within the OFDFT CINEB calculations: fixed and mixed boundary conditions (Fig. 1).

The $\frac{1}{2}\langle 110\rangle\{111\}$ dislocations in fcc metals typically separate into two $\frac{1}{6}\langle 112\rangle\{111\}$ Shockley partials in their equilibrium states. The present OFDFT simulations predict the spacing between these partials (the dislocation width) to be 10.9 Å (screw) and 20.4 Å (edge). The CINEB calculation for the edge dislocation with the fixed boundary condition does not show a clear energy barrier for dislocation motion. We therefore employ the mixed boundary condition explained in Sec. II to fairly compare the Peierls barriers for the screw and edge dislocations. On the basis of the CINEB results shown in Fig. 2 and using Eqs. (3) and (4), we predict σ_p for Al screw and edge dislocations to be 9.9 MPa ($3.0 \times 10^{-4}G$) and 1.6 MPa ($4.9 \times 10^{-5}G$), respectively (Table II). The shear modulus, relating stress and strain along a $\langle 110\rangle$ direction on a $\{111\}$ plane, is evaluated within OFDFT to be $G = \frac{(C_{44}+C_{11}-C_{12})}{3} = 32.7$ GPa (with $C_{11} = 114.9$ GPa, $C_{12} = 62.8$ GPa, and $C_{44} = 46.0$ GPa). We then verified those CINEB predictions by quasistatic loading simulations using the same mixed boundary condition. The latter method predicts 11.4 ± 1.6 MPa ($3.5 \pm 0.5 \times 10^{-4}G$) and 1.8 ± 0.2 MPa ($5.5 \pm 0.5 \times 10^{-5}G$) for screw and edge dislocations, respectively. The range of values corresponds to the uncertainty in the strain increment $\Delta\varepsilon$. The two different simulation methods with the same boundary condition predict nearly the same σ_ps for each dislocation. Both simulations predict around six times larger σ_p for the screw dislocation,

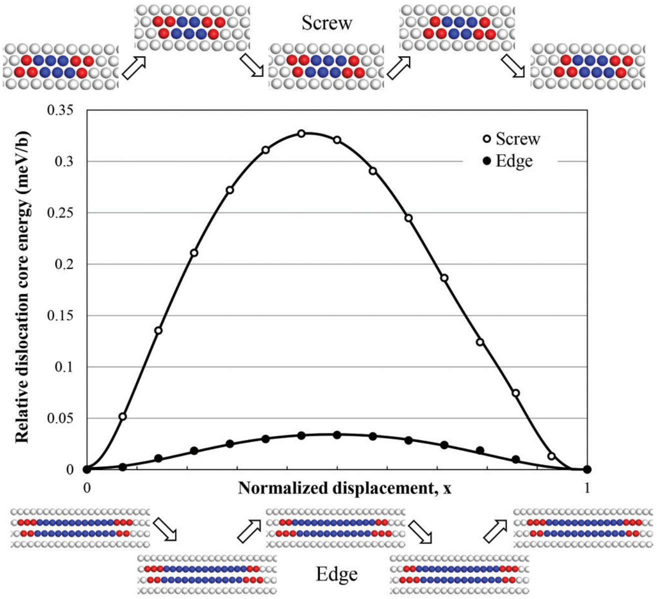

FIG. 2. (Color online) Variation of the relative dislocation core energies $E_C(x)$ for screw and edge dislocations [calculated using the CINEB method with the mixed boundary condition of Fig. 1(b)] as a function of the normalized displacement x traveled by the dislocation core. The energy unit is meV/b where b is the Burgers vector. Insets show corresponding atomic configurations of the screw (upper inset) and the edge (lower inset) dislocation cores along the MEP. Atoms are superimposed on the XY plane noted in Table I. Gray, blue, and red spheres indicate atoms locally in fcc, hcp, and unknown crystal structures, respectively, as derived from CNA. (Partial) dislocation core positions are determined as the center of "unknown structure" atoms (red). Between the partial dislocation cores lies an hcp stacking fault region (blue). The same convention is used in Fig. 4.

implying that the screw dislocation moves less readily than the edge dislocation. This result is also qualitatively predicted by its smaller width between partial cores.

In the mixed boundary simulation, an image force may exist on the free boundary surface that could pull the subsurface dislocation toward the surface. This force can be estimated as $\sigma_{img} \sim Gx^2/\pi d^2$ as the isolated single dislocation moves by one unit vector x along the glide plane (Sec. II). In our quasistatic loading simulation for the edge dislocation, $x = 1.4$ Å and the cell dimension $d = \sim 120$ Å so that $\sigma_{img} = \sim 1.4$ MPa. Since the image force is of the same order of magnitude as the calculated σ_p for the edge dislocation, the latter value may be questionable. However, in the CINEB calculation, the image force is essentially corrected by the last term on the right-hand side of Eq. (2).[67] The two different simulation methods predict nearly the same σ_p, which implies the image force was negligible in our quasistatic loading simulation with the mixed boundary condition. For the screw dislocation, the two simulation methods predict almost the same σ_p as well, and this σ_p is much larger than the image force. Thus, the results for the screw dislocation should be reliable. We also predict a σ_p of 6.2 MPa ($1.9 \times 10^{-4}G$) for the screw dislocation based on the fixed boundary CINEB calculation, in which no image force error exists. We see that the fixed boundary condition predicts a somewhat smaller σ_p than the mixed boundary condition, though it is still significantly larger than the σ_p for the edge dislocation so that qualitative trends remain unchanged.

The CINEB calculations also provide structures along the MEP for moving a dislocation, revealing the mechanism of motion. For the screw dislocation (Fig. 2, upper inset), the trailing partial core moves first, decreasing the SF region between the partials, then the leading partial core starts to move before the trailing one arrives in its equilibrium position, in an overall caterpillar motion. For the edge dislocation (Fig. 2, lower inset), the leading partial core moves first, increasing the SF region between the partials, and then the trailing partial core follows. The widths of both dislocations at the top of the barrier are the same as the equilibrium widths. Thus, we predict that at least in Al and perhaps in all fcc metals, partials do not move simultaneously; rather, one moves first, thereby providing the impetus to push or drag the other partial afterward. The different strain fields of the screw vs edge dislocations are probably responsible for why the order of partial dislocation motion (which one moves first) is not the same for the two dislocation types.

2. *Discussion*

We now compare our predictions to measurements so as to determine the accuracy of our OFDFT simulations (Table III). The kink pair formation mechanism, related to the Bordoni peak as discussed earlier, is widely believed responsible for the mobility of screw dislocations.[5,68] We therefore first compare the calculated σ_ps of the screw dislocation to those derived from the Bordoni relaxation peak of internal friction measurements. This Al σ_p is estimated to be

TABLE II. OFDFT Peierls stresses (σ_ps) for edge and screw dislocations in fcc Al using two different simulation methods and two different boundary conditions.

Simulation method	Boundary condition	Dislocation	σ_p (MPa)[a]
CINEB MEP calculation	Fixed	Edge (dissociated)	No energy barrier observed
		Screw (dissociated)	6.2 ($1.9 \times 10^{-4}G$)
		Screw (undissociated)	355 ($1.1 \times 10^{-2}G$)
	Mixed	Edge (dissociated)	1.6 ($4.9 \times 10^{-5}G$)
		Screw (dissociated)	9.9 ($3.0 \times 10^{-4}G$)
Quasistatic loading simulation	Mixed	Edge (dissociated)	1.8 ± 0.2 ($5.5 \pm 0.5 \times 10^{-5}G$)
		Screw (dissociated)	11.4 ± 1.6 ($3.5 \pm 0.5 \times 10^{-4}G$)

[a] G is the OFDFT-calculated shear modulus, 32.7 GPa, along a ⟨110⟩ direction on a {111} plane.

TABLE III. Calculated and measured Peierls stresses (σ_ps) for screw and edge dislocations in fcc Al.

Method	References	Screw σ_p (MPa)	Edge σ_p (MPa)
OFDFT simulation	This work[a]	6.2, 9.9, 355[b]	1.6
Internal friction measurement	Kosugi and Kino[9]	0.68	
	Koizumi *et al.*[10]	1.4	
	Various[5–8,c]	25∼250[d]	
Mechanical deformation test	Seeger and Schiller[4]	0.25∼2.5[e]	
Initial flow stress	Howe *et al.*[69]		1.06
	Wang[70]		0.71
EAM simulation	Bulatov *et al.*[16]	82	
	Lu *et al.*[17]	82	
	Fang and Wang[18,f]		2.3
	Olmsted *et al.*[19]	14–18	2
	Pasianot and Moreno-Gobbi[20]	35, 66	
	Srinivasan *et al.*[21,f]	1	1, 13[g], 225[b,g]
	Tsuru *et al.*[23]	39	1.75
PN-based model calculation	Lu *et al.*[17]	256, 88[h]	3.2, 24[h]
	Lu *et al.*[25]	256	
	Lu and Kaxiras[26]	254, 20[i]	2.9, 1.4[i]
	Hartford *et al.*[24]		0.9

[a] CINEB results listed again for comparison (from Table II).

[b] Undissociated core structure (for all other simulations, a dissociated core structure was modeled).

[c] Fantozzi *et al.* (Ref. 5), Benoit *et al.* (Ref. 6), Bujard *et al.* (Ref. 7), and Nabarro (Ref. 8).

[d] Generally reported as 10^{-2}–10^{-3} in the unit of shear modulus, which is ∼25 GPa (Ref. 27).

[e] Generally reported as 10^{-4}–10^{-5} in the unit of shear modulus.

[f] MD results within EAM (unless noted, the rest are molecular statics simulations).

[g] Baskes *et al.*'s EAM potential (Ref. 72) was used (for all other EAM simulations, Ercolessi-Adams potential (Ref. 71) was used).

[h] EAM GSFE was used within a PN-based model calculation (unless noted, KSDFT GSFE was used).

[i] Dislocation model includes vacancies (for all other simulations, vacancies were not included).

10^{-2}–$10^{-3}G$,[5–8] corresponding to the Bordoni relaxation peak between ∼100 and ∼200 K.[5] More recently, Kosugi and Kino[9] and Koizumi *et al.*[10] found a lower-temperature peak below 20 K with ultra–high-purity, zone-refined Al single crystals (impurity concentration of ∼1 ppm), corresponding to σ_ps of $2.7 \times 10^{-5}G$ and $5.4 \times 10^{-5}G$, respectively. Since most theoretical simulations (including ours) model a dislocation in a pure Al single crystal, such predictions should be compared to Kosugi and Kino's[9] and Koizumi *et al.*'s[10] measurements. Our OFDFT simulation predicts somewhat larger σ_ps: 6.2 MPa ($1.9 \times 10^{-4}G$) or 9.9 MPa ($3.0 \times 10^{-4}G$) based on the fixed or mixed boundary CINEB calculations, respectively. However, our values are much closer to the experimental σ_p estimated from the lower-temperature Bordoni peak[9,10] than all but one previous simulation[21] (Table III, *vide infra*). The σ_p based on the fixed boundary condition shows slightly better agreement with the experimental σ_p. We use this value for comparison to the σ_p of the undissociated screw dislocation in the next section, for which we use only the (more accurate) fixed boundary condition. Our result also agrees well with mechanical deformation tests (10^{-4}–$10^{-5}G$).[4] In such critical resolved shear stress measurements, screw dislocation mobility is considered to be the determining factor, rather than its edge counterpart, due to the former's lower mobility. Our predicted mobility of an edge dislocation, σ_p of ∼1.6 MPa ($4.9 \times 10^{-5}G$) from both CINEB and quasistatic loading simulations, is in good agreement with experimental values for edge dislocation motion estimated from initial flow stresses, e.g., 1.06 MPa (Ref. 69) and 0.71 MPa (Ref. 70).

In principle, OFDFT should be the most robust theoretical method for calculating σ_p in metals used to date because it simultaneously considers QM effects and atomic relaxations for thousands of atoms around the dislocation core. Comparison to experiment verifies its accuracy. We next compare our OFDFT results to those from other theoretical methods (Table III). For the screw dislocation, all EAM simulations but one predicted much larger values than our OFDFT predictions, yielding larger disagreement with the experimental σ_p estimated from the lower-temperature Bordoni peak.[9,10] All of these EAM simulations employed the Ercolessi-Adams potential,[71] generally considered to be the most reliable EAM potential for Al. Srinivasan *et al.* predicted a smaller σ_p of 1 MPa for both screw and edge dislocations from MD simulations[21]; however, the σ_p values for both types of dislocations were predicted to be the same, which points to a problem with these MD simulations. Lu *et al.* predicted a much larger value of 256 MPa based on the semi-discrete PN model,[17,25,26] which differs by two orders of magnitude compared to σ_p estimated from the lower-temperature Bordoni peak. For the edge dislocation, our OFDFT result agrees well with both the EAM simulation results and PN-based model calculations that employed a KSDFT GSFE. However, an order of magnitude larger σ_p for an edge dislocation of 13 MPa was derived from Srinivasan *et al.*'s MD simulation[21] that employed a different EAM potential.[72] This may be attributed to the quality of this EAM potential, which is less accurate than the Ercolessi-Adams potential[71] for evaluating SFEs. Finally, Lu *et al.*'s PN-based model calculation employing an EAM GSFE predicts a σ_p for an edge dislocation of 24 MPa.[17] This significantly overestimated value is due to the less accurate EAM GSFE compared to the KSDFT one. This comparison of σ_p values leads us to conclude that QM simulation methods are needed to accurately model the motion of Al dislocations.

B. Peierls stress of an undissociated screw dislocation in fcc Al

1. Results

As the last section demonstrated, OFDFT CINEB simulations provide accurate σ_ps for screw and edge dislocations in Al. By considering both QM and atomic relaxation effects simultaneously, we can now address the discrepancy between σ_p values estimated from mechanical tests and the lower-temperature Bordoni peak (10^{-4}–$10^{-5}G$) compared to those from the typical, higher-temperature Bordoni peak (10^{-2}–$10^{-3}G$).

During structural optimization of the screw dislocation starting with the initial conditions given in Sec. II, we unexpectedly discovered a metastable, undissociated core structure where the maximum force component on any atom is less than 10.5 meV/Å (Fig. 3), suggesting a metastable state that may exist before partial dislocations are formed. We find that the peak in the maximum force component between the undissociated (point A) and the dissociated (point B) cores is due to core atoms only. Forces on atoms near the boundaries do not change noticeably throughout the optimization. This undissociated core structure has not been reported in any previous simulation, and our own EAM test calculations using the classical Ercolessi-Adams potential[71] do not find this structure. This means the metastable, undissociated core exists due to subtle QM effects—electron density fluctuations—inherent in the screw dislocation. By contrast, no undissociated structures are found by OFDFT for the edge dislocation, just as expected by elasticity theory.[50] As mentioned earlier, the difference in dislocation core widths predicted by OFDFT (small for screw and large for edge), coupled with elasticity theory thresholds for dissociation, is consistent with these findings. Recall that both OFDFT and EAM simulations agreed well for the σ_p of an edge dislocation; however, the OFDFT-calculated σ_p for a screw dislocation showed much better agreement than EAM when comparing to experimental estimations from the lower-temperature Bordoni peak (Sec. III A).

We then investigated the behavior of this undissociated screw dislocation using OFDFT CINEB simulations to calculate its σ_p for comparison with the dissociated screw dislocation σ_p. Along its MEP (Fig. 4, upper inset), the undissociated core starts to move by broadening along the glide direction, becoming widest at the top of the barrier. After the barrier, the core starts to narrow. This motion is contrary to its dissociated counterpart, which starts to move

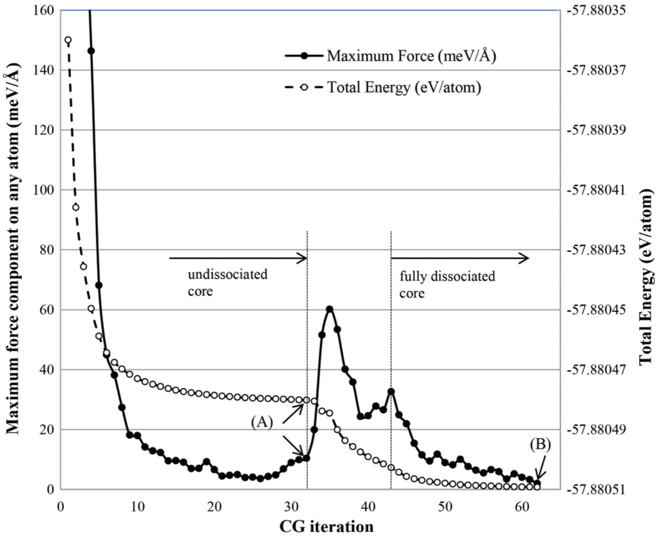

FIG. 3. Maximum force component and total energy per atom as a function of CG iteration steps for the screw dislocation structure optimization. Quick minimization (Ref. 78) and Broyden-Fletcher-Goldfarb-Shanno (Ref. 79) algorithms also predict the same results as CG minimization. Unlike the maximum force component, the total energy always decreases as iterations proceed. Until the first vertical line, the dislocation core remains undissociated. Point A indicates the lowest energy structure for the undissociated core. Beyond point A, the dislocation starts to dissociate into partials. After the second vertical line, the dislocation core fully dissociates. At the final iteration indicated by point B, we obtain the optimized, fully dissociated partial dislocation core structure.

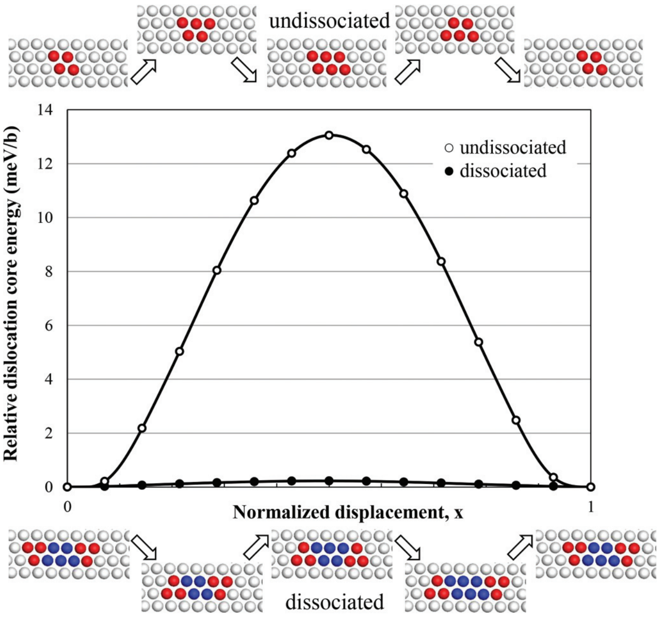

FIG. 4. (Color online) Variation of the relative dislocation core energies $E_C(x)$ for dissociated and undissociated screw dislocations [calculated using the CINEB method with the fixed boundary condition of Fig. 1(a)] as a function of normalized displacement x traveled by the dislocation core. The energy unit is meV/b where b is the Burgers vector. Insets show corresponding atomic configurations of the undissociated (upper inset) and the dissociated (lower inset) screw dislocation along the MEP.

by shortening the width between partial cores (Fig. 4, lower inset). As mentioned above, the σ_p of the dissociated screw dislocation is predicted to be 6.2 MPa ($1.9 \times 10^{-4}G$). For the undissociated core, we predict a σ_p of 355 MPa ($1.1 \times 10^{-2}G$), consistent with the two orders of magnitude discrepancy in σ_p measurements in fcc metals. Our work suggests that both dissociated and undissociated cores can exist in Al at both low and high temperature. At low temperature, the only motion will be of dislocations that can move easily, while at higher temperature, dislocations that are harder to move will do so as well. The smaller σ_p for the dissociated dislocation corresponds to the lower-temperature (<20 K) Bordoni peak observed in ultra–high-purity samples,[9,10] since a lower energy cost is incurred to form a kink pair by moving a segment of a dislocation line. The larger σ_p for the undissociated dislocation corresponds to the (typical) higher-temperature (between ∼100 and ∼200 K) Bordoni peak,[5–8] since it needs to overcome a larger energy barrier to move. We suggest that the undissociated screw dislocations may exist intrinsically or may be further stabilized by impurity pinning.

2. *Discussion*

These results provide the first evidence that partially supports Takeuchi's earlier hypothesis.[73] Takeuchi first assumed that most dislocations in the dislocation network produced by annealing do not lie on $\{111\}$ glide planes (dislocations skewed from the glide plane by $>10^\circ$ do not dissociate[73]). Takeuchi then proposed that the typical Bordoni peak in annealed and deformed fcc metals corresponding to the σ_p of 10^{-2}–$10^{-3}G$ could be attributed to the motion of undissociated dislocations. Takeuchi did not present experimental or simulation data to test this assumption; the idea that dislocation dissociation is the origin of the σ_p discrepancy in fcc metals has been confirmed by our simulations. Unlike Takeuchi's interpretation, however, our OFDFT simulation suggests the undissociated screw dislocation, in addition to the dissociated one, may exist on $\{111\}$ glide planes.

Clearly, impurities play a key role in determining the σ_p in fcc metals. Kosugi and Kino determined that keeping straight dislocation segments along the Peierls valley (where the dislocation line resides in its equilibrium configuration) requires the pinning distance to be larger than 10^{-3} cm; otherwise, kinks will overlap and dislocation lines will become tangled. Thus, impurity concentrations must be controlled within parts per million (ppm).[9] Unfortunately, this cannot be tested directly in simulations, since atomic simulations, even within EAM, are not feasible for pinned dislocation segments larger than 10^{-3} cm with ppm order impurities. However, our first-principles OFDFT simulations suggest that metastable, undissociated dislocations may exist in typical Al samples with impurity concentrations larger than the ppm level, since these simulations find a difference of two orders of magnitude in σ_p for dissociated vs undissociated cores. Our results further suggest that the impurities are responsible for preventing dissociation of the screw dislocations.

Srinivasan *et al.* also suggested that this discrepancy could be attributed to dislocation dissociation,[21] but the proposal was based on faulty reasoning. Using MD simulations with Baskes *et al.*'s EAM potential,[72] they predicted σ_ps of 13 and 225 MPa, respectively, for dissociated and undissociated edge dislocations. However, perfect edge dislocations cannot give rise to a Bordoni relaxation because they cannot form kink pairs in the temperature domain of the Bordoni peak.[5,68] Moreover, the authors did not observe such changes in the σ_p for screw dislocations, as they should have. Furthermore, the more widely-used, higher-quality Ercolessi-Adams potential[71] does not predict an undissociated configuration for either the screw or the edge dislocations. We therefore dismiss these earlier findings as not well founded.

A vacancy lubrication effect has been suggested as an alternative origin of the σ_p discrepancy in fcc metals.[74,75] Lu and Kaxiras predicted σ_ps of 254 and 20 MPa for screw dislocations without and with vacancies, respectively, based on the semi-discrete PN calculation with KSDFT GSFE.[26] However, their simulation model contained 4% vacancies, which is a much larger concentration than typical experimental specimens contain (ppm). Although the vacancy concentration at the dislocation core will be larger than the average bulk value due to local stress-induced reduction in the vacancy formation energy, it seems unlikely that the vacancy concentration will be four orders of magnitude higher than the bulk value. Because the actual vacancy concentrations at dislocation cores are not known, it remains an open question as to whether potentially vastly lower concentrations of vacancies in a real sample could lead to such lubrication.

IV. CONCLUSIONS

We have investigated Al dislocation motion via OFDFT simulations. This method provides σ_p values with first-principles accuracy. To the best of our knowledge, these first-principles σ_p values calculated from atomic-scale simulations are the first reported for Al. For the equilibrium configurations of screw and edge dislocations in which they separate into Shockley partials, OFDFT predicts σ_ps of $\sim 10^{-4}$–$10^{-5}G$, in good agreement with those estimated from mechanical deformation tests and a lower-temperature Bordoni relaxation peak. The approximately six times smaller σ_p of the edge dislocation implies edge dislocations move more readily than do screw dislocations, as expected from the former's larger width. OFDFT also predicts a metastable configuration for a screw dislocation in which the core remains undissociated. For this structure, OFDFT predicts σ_p of $\sim 10^{-2}$–$10^{-3}G$, in good agreement with those estimated from the typical, higher-temperature Bordoni relaxation peak. By comparing the values obtained from the dissociated vs undissociated screw dislocations, we have successfully reproduced the differences of two orders of magnitude for measured σ_ps in fcc metals. Kosugi and Kino attributed their smaller σ_p (10^{-4}–$10^{-5}G$) to the use of a high-purity Al sample.[9] We therefore conclude that the difference in screw dislocation configurations, i.e., a dissociated core in a high-purity crystal vs an undissociated core induced by impurities in a typical crystal, is the most likely origin of the σ_{p} discrepancy in fcc metals.

The metastable, undissociated screw dislocation structure has only been obtained using a method that accounts for QM effects, i.e., OFDFT. This suggests that transferable and accurate QM methods are necessary to reliably calculate dislocation structures and motion, even in a pure single crystal. If we consider more complicated material properties, e.g., vacancy effects on dislocation behavior, dislocations in metal alloys, and dislocation interactions with other defects, accurate QM methods are likely to be even more important to use. Although OFDFT is inexpensive yet accurate enough compared to standard KSDFT to be applied to dislocation simulations in simple metals like Al, its current computational cost still precludes, e.g., long MD trajectories with millions of atoms. In addition, the nearly-free-electron response function used to derive most nonlocal KEDFs still hinders its general application to other types of materials (though recent advances hold promise[76,77]). Nevertheless, OFDFT can play a useful role in providing insight into characterizing the properties of novel main group metals and their alloys.

ACKNOWLEDGMENTS

We are grateful to the Office of Naval Research for funding this work. Princeton University and the U.S. Department of Defense supercomputing resource center are thanked for supercomputing time. We also thank Dr. Mohan Chen and Dr. John A. Keith for critically reading the manuscript.

---

[*] Corresponding author: eac@princeton.edu

[1] J. P. Hirth and J. Lothe, *Theory of Dislocations*, 2nd ed. (John Wiley & Sons, New York, 1982).

[2] P. G. Bordoni, Ric. Sci. **19**, 851 (1949); J. Acoust. Soc. Am. **26**, 495 (1954).

[3] A. Seeger, Philos. Mag. **1**(7), 651 (1956).

[4] A. Seeger and P. Schiller, in *Physical Acoustics*, edited by W. Mason (Academic Press, New York, 1966), Vol. 3, p. 366.

[5] G. Fantozzi, C. Esnouf, W. Benoit, and I. G. Ritchie, Prog. Mater. Sci. **27**, 311 (1982).

[6] W. Benoit, M. Bujard, and G. Gremaud, Phys. Status Solidi A **104**, 427 (1987).

[7] M. Bujard, G. Gremaud, and W. Benoit, J. Appl. Phys. **62**, 3173 (1987).

[8] F. R. N. Nabarro, Philos. Mag. A **75**(3), 703 (1997).

[9] T. Kosugi and T. Kino, J. Phys. Soc. Jpn. **58**, 4269 (1989).

[10] H. Koizumi, T. Koizumi, and T. Kosugi, J. Alloys Compd. **310**, 107 (2000).

[11] R. E. Peierls, Proc. Phys. Soc. London **52**, 23 (1940).

[12] F. R. N. Nabarro, Proc. Phys. Soc. London **59**, 256 (1947).

[13] M. S. Daw and M. I. Baskes, Phys. Rev. Lett. **50**, 1285 (1983).

[14] M. S. Daw and M. I. Baskes, Phys. Rev. B **29**, 6443 (1984).

[15] W. Kohn and L. J. Sham, Phys. Rev. **140**, A1133 (1965).

[16] V. V. Bulatov, O. Richmond, and M. V. Glazov, Acta Mater. **47**, 3507 (1999).

[17] G. Lu, N. Kioussis, V. V. Bulatov, and E. Kaxiras, Phys. Rev. B **62**, 3099 (2000).

[18] Q. F. Fang and R. Wang, Phys. Rev. B **62**, 9317 (2000).

[19] D. L. Olmsted, K. Y. Hardikar, and R. Phillips, Model. Simulat. Mater. Sci. Eng. **9**, 215 (2001).

[20] R. C. Pasianot and A. Moreno-Gobbi, Phys. Status Solidi B **241**, 1261 (2004).

[21] S. G. Srinivasan, X. Z. Liao, M. I. Baskes, R. J. McCabe, Y. H. Zhao, and Y. T. Zhu, Phys. Rev. Lett. **94**, 125502 (2005).

[22] Y. Liu, G. Lu, Z. Chen, and N. Kioussis, Model. Simulat. Mater. Sci. Eng. **15**, 275 (2007).

[23] T. Tsuru, Y. Kaji, and Y. Shibutani, J. Comput. Sci. Tech. **4**, 185 (2010).

[24] J. Hartford, B. von Sydow, G. Wahnström, and B. I. Lundqvist, Phys. Rev. B **58**, 2487 (1998).

[25] G. Lu, N. Kioussis, V. V. Bulatov, and E. Kaxiras, Mater. Sci. Eng. A **309-310**, 142 (2001).

[26] G. Lu and E. Kaxiras, Phys. Rev. Lett. **89**, 105501 (2002).

[27] H. B. Huntington, Solid State Phys. **7**, 213 (1958).

[28] L. Hung and E. A. Carter, Model. Simulat. Mater. Sci. Eng. **19**, 045002 (2011).

[29] L. Hung and E. A. Carter, Chem. Phys. Lett. **475**, 163 (2009).

[30] D. R. Bowler, J. L. Fattebert, M. J. Gillan, P. D. Haynes, and C. K. Skylaris, J. Phys.: Condens. Matter **20**, 290301 (2008).

[31] F. Shimojo, R. K. Kalia, A. Nakano, K. Nomfura, and P. Vashishta, J. Phys. Condens. Matter **20**, 294204 (2008); A. Nakano, R. K. Kalia, K. Nomura, A. Sharma, P. Vashishta, F. Shimojo, A. C. T. van Duin, W. A. Goddard, R. Biswas, D. Srivastava, and L. H. Yang, Int. J. High Perform. Comp. Appl. **22**, 113 (2008); F. Shimojo, R. K. Kalia, A. Nakano, and P. Vashishta, Phys. Rev. B **77**, 085103 (2008).

[32] S. C. Watson and P. A. Madden, PhysChemComm **1**, 1 (1998).

[33] Y. A. Wang and E. A. Carter, in *Condensed Phase Chemistry*, Progress in Theoretical Chemistry and Physics, edited by S. D. Schwartz (Kluwer, Dordrecht, the Netherlands, 2000), p. 117.

[34] S. C. Watson and E. A. Carter, Comput. Phys. Comm. **128**, 67 (2000).

[35] G. Ho, C. Huang, and E. A. Carter, Curr. Opin. Solid State Mater. Sci. **11**, 57 (2007).

[36] L.-W. Wang and M. P. Teter, Phys. Rev. B **45**, 13196 (1992).

[37] M. Foley and P. A. Madden, Phys. Rev. B **53**, 10589 (1996).

[38] Y. A. Wang, N. Govind, and E. A. Carter, Phys. Rev. B **60**, 16350 (1999); **64**, 089903(E) (2001).

[39] C. Huang and E. A. Carter, Phys. Rev. B **81**, 045206 (2010).

[40] B. Zhou, Y. A. Wang, and E. A. Carter, Phys. Rev. B **69**, 125109 (2004).

[41] C. Huang and E. A. Carter, Phys. Chem. Chem. Phys. **10**, 7109 (2008).

[42] I. Shin and E. A. Carter, Model. Simulat. Mater. Sci. Eng. **20**, 015006 (2012).

[43] B. J. Jesson and P. A. Madden, J. Chem. Phys. **113**, 5924 (2000).

[44] K. M. Carling and E. A. Carter, Model. Simulat. Mater. Sci. Eng. **11**, 339 (2003).

[45] D. J. Gonzalez, L. E. Gonzalez, and M. J. Stott, Phys. Rev. B **74**, 014207 (2006).

[46] G. Ho, M. T. Ong, K. J. Caspersen, and E. A. Carter, Phys. Chem. Chem. Phys. **9**, 4951 (2007).

[47] G. Ho and E. A. Carter, J. Comput. Theo. Nanos. **6**, 1236 (2009).

[48] I. Shin, A. Ramasubramaniam, C. Huang, L. Hung, and E. A. Carter, Philos. Mag. **89**(34–36), 3195 (2009).

[49] L. Hung and E. A. Carter, J. Phys. Chem. C **115**, 6269 (2011).

[50] S. Takeuchi, Mater. Sci. Eng. A **400-401**, 84 (2005).

[51] G. Henkelman, G. Johannesson, and H. Jónsson, J. Chem. Phys. **113**, 9901 (2000).
[52] G. Henkelman, G. Jóhannesson, and H. Jónsson, Prog. Theor. Chem. Phys. **5**, 269 (2002).
[53] G. Ho, V. L. Ligneres, and E. A. Carter, Comput. Phys. Comm. **179**, 839 (2008); L. Hung, C. Huang, I. Shin, G. Ho, V. L. Ligneres, and E. A. Carter, *ibid.* **181**, 2208 (2010).
[54] D. M. Ceperley and B. J. Alder, Phys. Rev. Lett. **45**, 566 (1980).
[55] J. P. Perdew and A. Zunger, Phys. Rev. B **23**, 5048 (1981).
[56] L. E. Murr, *Interfacial Phenomena in Metals and Alloys* (Addison Wesley, Reading, MA, 1975).
[57] I. L. Dillamore and R. E. Smallman, Philos. Mag. **12**(115), 191 (1965).
[58] R. E. Smallman and P. S. Dobson, Metall. Trans. **1**, 2383 (1970).
[59] M. J. Mills and P. Stadelmann, Philos. Mag. A **60**(3), 355 (1989).
[60] N. Troullier and J. L. Martins, Phys. Rev. B **43**, 1993 (1991).
[61] See Supplemental Material at http://link.aps.org/supplemental/10.1103/PhysRevB.88.064106 for more boundary condition tests.
[62] W. Höllerbauer and H. P. Karnthaler, Beitr. Elektronenmikroskop. Direktabb. Oberfl. **14**, 361 (1981).
[63] D. Rodney, Acta Mater. **52**, 607 (2004); S. Groh, E. B. Martin, M. F. Horstemeyer, and D. J. Bammann, Model. Simulat. Mater. Sci. Eng. **17**, 075009 (2009); J. A. Yasi, T. Nogaret, D. R. Trinkle, Y. Qi, L. G. Hector, and W. A. Curtin, *ibid.* **17**, 055012 (2009).
[64] G. Wang, A. Strachan, T. Çağin, and W. A. Goddard III, Model. Simulat. Mater. Sci. Eng. **12**, S371 (2004).
[65] H. Tsuzuki, P. S. Branicio, and J. P. Rino, Comput. Phys. Comm. **177**, 518 (2007).
[66] S. Plimpton, J. Comput. Phys. **117**, 1 (1995).
[67] In an infinitely large cell (where we can ignore artificial boundary effects such as the image force), energies of the first and last CINEB images will be the same because of periodicity of the crystal. In a finite-sized cell (which may have artificial boundary effects), energies of the first and last CINEB images can be different (i.e., $E_{CINEB}(L)$ and $E_{CINEB}(0)$ in Eq. (2)) because distances from the boundary are different. However, this energy difference can be corrected in Eq. (2) when calculating the relative dislocation core energy $E_C(x)$.
[68] A. Seeger, J. Phys. **32**, C2-193 (1971).
[69] S. Howe, B. Liebmann, and K. Lucke, Acta Metall. **9**, 625 (1961).
[70] J. N. Wang, Acta Mater. **44**, 855 (1996).
[71] F. Ercolessi and J. B. Adams, Europhys. Lett. **26**, 583 (1994).
[72] M. I. Baskes, J. E. Angelo, and N. R. Moody, in *Hydrogen Effects in Materials*, edited by A. W. Thompson and N. R. Moody (Minerals, Metals and Materials Society, Warrendale, PA, 1996), p. 77.
[73] S. Takeuchi, J. Phys. Soc. Jpn. **64**, 1858 (1995).
[74] J. Lauzier, J. Hillairet, A. Vieux-Champagne, and W. Benoit, J. Phys. Condens. Matter **1**, 9273 (1989); J. Lauzier, J. Hillairet, G. Gremaud, and W. Benoit, *ibid.* **2**, 9247 (1990).
[75] W. Benoit, G. Gremaud, and B. Quenet, Mater. Sci. Eng. A **164**, 42 (1993).
[76] C. Huang and E. A. Carter, Phys. Rev. B **85**, 045126 (2012).
[77] J. Xia and E. A. Carter, Phys. Rev. B **86**, 235109 (2012).
[78] I. Stich, R. Car, M. Parrinello, and S. Baroni, Phys. Rev. B **39**, 4997 (1989); M. J. Gillan, J. Phys. Condens. Matter **1**, 689 (1989); G. Kresse and J. Furthmüller, Comput. Mater. Sci. **6**, 15 (1996); Phys. Rev. B **54**, 11169 (1996).
[79] R. H. Byrd, P. Lu, J. Nocedal, and C. Zhu, SIAM J. Sci. Comput. **16**, 1190 (1995).